

ORIGINAL ARTICLE

Open Access



Microstructure evolution and tribo-oxidation induced by friction and wear of cast iron brake discs

Quanshun Luo^{1*} , Jing Shen², Xudong Wang², Nick Farmilo¹ and Xiuhua Guo^{1,3}

Abstract

Braking discs play an important role for the safety of vehicles whereas severe frictional contacts in repeated braking operations result in thermal and tribological failures. This paper reports comprehensive surface and subsurface analyses of a used grey cast iron braking disc to investigate its failure mechanisms as well as related microstructure evolution. Thermal cracking, spalling wear and tribo-oxidation have been found to contribute to the wear failure. The flake-type graphite of the grey cast iron triggered propagation and internal oxidation of the metallic matrix. In a depth of 3 mm beneath the rubbing surface, extensive microstructure evolution occurred by severe plastic deformation of the ferritic matrix, nodularisation and partial dissolution of the lamellar carbides, and internal oxidation. The microstructure evolution resulted in decreased surface hardness to HV_{0.3} 247 as compared to HV_{0.3} 284 of the bulk cast iron.

Keywords Braking discs, Grey cast iron, Frictional heating, Worn surface analysis, Tribo-oxidation, Thermal cracking

1 Introduction

In automotive vehicles, the braking system, consisting of a brake rotor or disc and a brake pad, is the essential safety unit to control the vehicle speed and to ensure the safety of the driver and the passengers [1–5]. In a braking process, the static brake pad pulls to the rotating brake disc to generate a frictional resistance so that the rotation speed of the disc, and consequently the moving speed of the vehicle, can be gradually reduced [1, 2, 6]. Depending on the applied braking force, the frictional resistance transforms the kinetic energy of the moving vehicle into friction heat energy of the braking system. Meanwhile, compressive and tangential stresses are applied on the disc-pad sliding contact. Consequently, the severe

mechanical and thermal loading conditions result in wear and cracking failures of the braking pad and disc [2, 5–11]. In addition to this, another concern has been addressed in terms of environment protection regarding the particulate matter (PM) generated in the disc-pad sliding contact [4, 12]. It was claimed that the PM10, i.e., particulate matter less than 10 μm size, generated in braking systems accounts for about 50% of overall non-exhaust wear emissions from vehicle transportation [4].

High-strength grey cast iron having microstructure of flake-like graphite and pearlitic matrix is the primary material to manufacture brake discs for road-based vehicles owing to the low production cost, sufficient strength property, good thermal conductivity and diffusion capability as well as vibration-absorbing capacity [1, 3, 6, 10, 13, 14]. Other ferrous alloys, such as spheroidal graphite cast irons and low-alloy steels, are used to produce brake rotors of railway cars [8, 9, 11, 15]. Although other light-weight materials with superior corrosion resistance are being developed, such as aluminium-matrix composites, titanium alloys and fibre-strengthened carbon

*Correspondence:

Quanshun Luo
q.luo@shu.ac.uk

¹ Materials and Engineering Research Institute, Sheffield Hallam University, Sheffield, South Yorkshire, UK

² Firstlink Auto Parts Ltd, Sheffield, South Yorkshire, UK

³ School of Material Science and Engineering, Henan University of Science and Technology, Luoyang, Henan Province, China



© The Author(s) 2024. **Open Access** This article is licensed under a Creative Commons Attribution 4.0 International License, which permits use, sharing, adaptation, distribution and reproduction in any medium or format, as long as you give appropriate credit to the original author(s) and the source, provide a link to the Creative Commons licence, and indicate if changes were made. The images or other third party material in this article are included in the article's Creative Commons licence, unless indicated otherwise in a credit line to the material. If material is not included in the article's Creative Commons licence and your intended use is not permitted by statutory regulation or exceeds the permitted use, you will need to obtain permission directly from the copyright holder. To view a copy of this licence, visit <http://creativecommons.org/licenses/by/4.0/>.

composites, grey cast iron is still the most widely used disc material [4].

Up to date, most published research on failures of brake discs has been focused on the cracking and wear failures. Mackin reported cracking failures of a grey cast iron disc featuring the primary radial cracking across its radial section, networks of small circumferential cracks and thermal crackles, and wear induced surface deformation [6]. The radial cracking can be attributed to circumferential cyclic tensile-compressive stress and residual stresses caused by thermal shocks when the braking contacts caused increased surface temperature up to 900 °C. Similar thermal shocks of cast iron discs were also reported by other authors [1, 3, 7, 10]. Bagnoli also reported small-depth penetration of crackle cracks along graphite flakes [7]. He found that a crack of a grey cast iron disc showing a hot cracking failure initiated at a connecting claw followed by its propagation along graphite flakes [5]. Thermal shock cracking is also a major failure of other materials, such as brake discs of railway cars made from alloy steels and spheroidal cast irons [8, 9, 11, 15, 16].

Fundamental research on sliding wear of cast irons has also been published, e.g., in Refs [13, 14, 16]. Riahi published experimental results on sliding wear of grey cast iron samples against ball bearing steel that mild occurred at a combination of low load and low sliding speed with the formation of oxide-based tribofilms [14].

On the other hand, the increase of applied load or sliding speed caused transition to severe adhesive wear. König reported the significant influence of temperature on the wear mechanisms of grey cast iron that adhesive wear took place at temperatures lower than 400 °C whereas the wear at higher temperatures brought about the formation of a lubricious glaze layer of Fe_2O_3 -type oxide on the worn surface [16]. Other researchers reported Fe_3O_4 or Fe_2O_3 based tribofilms on the worn disc surfaces depending on different circumstances [16–18]. In view of wear induced microstructure changes, several researchers reported hardened worn surfaces accompanying the formation of gradient microstructure including extremely refined surface microstructure to various plastic deformation to certain depths [17, 19, 20]. However, there was little published research regarding the wear induced evolution of the pearlitic microstructure and its interaction with the graphite flake.

This paper reports comprehensive microstructure characterisation of a used brake disc. The grey cast iron disc was disassembled from a heavy-duty lorry after a radial cracking failure was detected, as shown in Fig. 1a. By means of optical and electron microscopic observations and spectroscopic and diffractometric analyses, wear induced decomposition, dissolution and plastic deformation of the pearlitic matrix microstructure were found. In addition to the formation of a Fe_3O_4 -type tribofilm, the

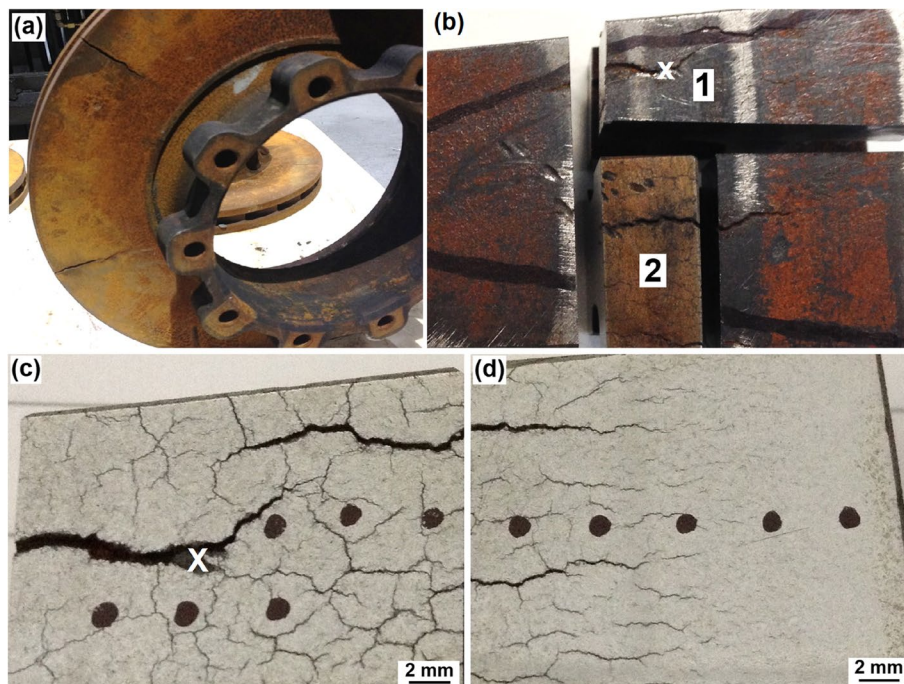


Fig. 1 Visual inspection of network cracking on the rubbing surface: **a** A photograph of the failed disc brake. **b** Sectioned blocks of the disc part. **c-d** Network cracking on the polished disc surface

graphite flakes were found to be a channel both for crack propagation and for internal oxidation. These microstructural evolutions contributed to decreased surface hardness.

1.1 Experimental

1.1.1 The failed brake rotor, cutting and subsequent preparation

Figure 1a is a photograph showing the failed brake rotor. The rotor has a double-disc sandwich structure to allow ventilation cooling of the rubbing discs. Several radial macro-cracks had already formed. Figure 1b shows the cutting strategy of a block taken from the failed rotor. The piece marked '1' was for analyses of the disc worn surface which contains various cracks. The piece marked '2' was used for cross-sectional analysis to examine penetration of surface cracks. After applying gentle grinding and polishing to remove the surface oxide layer of the rubbing surface marked '1', this piece is imaged in Fig. 1c and d where both macro radial cracks and network-like small cracks become visible. The black marks were made as position references for surface hardness testing.

1.2 Characterisations

Vickers microhardness profiles were measured both on the polished rubbing surface (as shown in Fig. 1c and d) and on the cross-sectional sample. A hardness tester Duramin-40 AC3 (STRUERS APS, Ballerup, Denmark)

was employed for the tests. A small indentation load of 0.3 kgf was selected to restrict the indentation depth so that the measured hardness values reflect the hardness of the rubbing surface.

A scanning electron microscope (SEM), FEI Nova 200 FEG-SEM instrument (FEI Europe BV, Eindhoven, The Netherlands) was employed to observe the worn surface and microstructure. The SEM instrument was attached with an energy dispersive X-ray (EDX) spectrometer, which was applied to determine the chemical compositions of the observed areas. The worn surface to be observed was cleaned using acetone with soft fibric tissue. The samples for microstructure observation were metallographically ground, polished and chemically etched using a 2% nital etchant. The non-etched samples were observed using an optical microscope (OPM) to characterise the graphite phase. An X-ray diffractometer with a copper anode (using Cu-K α radiation with wavelength $\lambda = 0.1456$ nm) was employed to analyse the worn surface.

2 Results

2.1 Characterisation of the grey cast iron disc

The microstructure of the cast iron disc was observed using optical and electron microscopic observations. Figure 2 shows optical microscopic observations prior to and after chemical etching. In Fig. 2a and b, the surface and core parts both show similar A-type flake-like

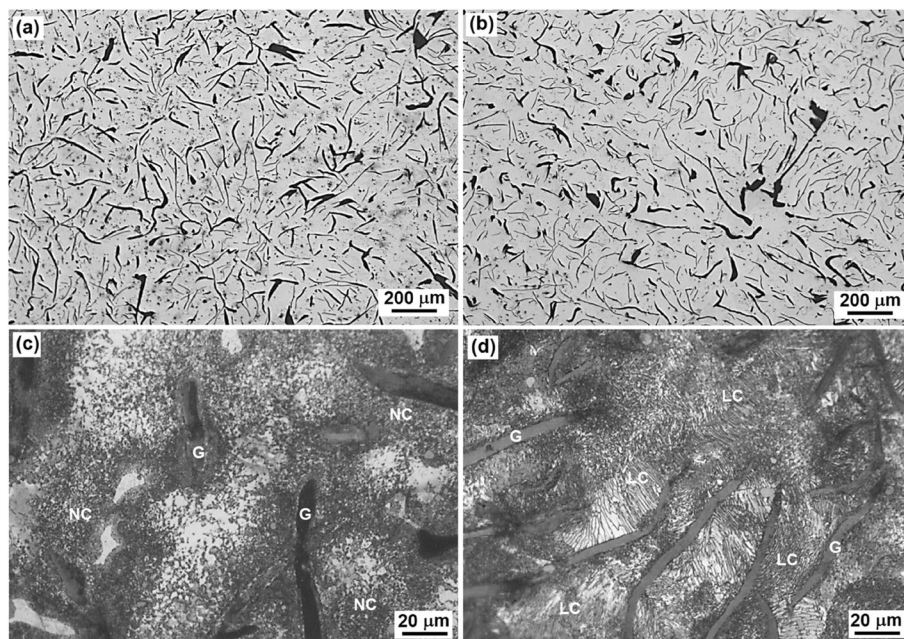


Fig. 2 Optical micrographs showing the microstructure of the grey cast iron disc: **a** A-type graphite flakes at a depth of 2 mm; **b** A-type graphite flakes at the core part; **c** Nodularised carbides in the matrix at a depth of 2 mm; and **d** pearlitic matrix in the core part. The marks 'G', 'NC' and 'LC' stand for graphite, nodularised carbides and lamellar carbides, respectively

graphite. The graphite flakes exhibit homogeneous distribution across the whole section. Such graphite characteristics, including its shape, quantity and distribution, are commonly seen in most cast iron disks for the provision of good thermal conductivity and dampening properties [1, 3, 4, 7, 12, 18]. Figure 2c and d show the pearlitic matrix microstructure after the sample was etched. In the whole section, the matrix comprises the ferritic matrix and cementite lamella, whereas no pre-eutectoid ferrite grain was observed. Figure 3 presents SEM images taken at a series of different magnifications showing the graphite distribution and details of the pearlitic carbide. Such pearlitic matrix is essential for high strength grey cast irons used in brake rotors or discs [1, 3, 5–7, 10, 14]. In this case, the hardness was measured to be $HV_1 223 \pm 5$ in the braking disc and $HV_1 210 \pm 24$ in the core of the rotor, respectively.

Moreover, the OPM and SEM observations revealed nodularisation of lamellar carbides in the pearlitic matrix adjacent to the rubbing surface. It can be seen in Fig. 2c that the carbide phase exhibits a nodularised shape differing from the typical lamellar morphology, which implies some kinds of microstructure evolution in small depths adjacent to the rubbing surface. Figure 3 also indicates some other evidences of the evolution. Firstly, the graphite flakes seem to have been enveloped each with a shell, as shown in Fig. 3b. In Fig. 3c, the shell has a clear interface separating itself from the pearlitic matrix. Secondly, Fig. 3b also shows some areas where the carbide constituents are nodular instead of pearlite. Such an important phenomenon was not reported in literature, to the best of our knowledge. More details of the microstructure evolution are shown in Sect. 3.3.

2.2 Analyses of disc worn surface

The rubbing surface was observed using SEM, Fig. 4. The smooth worn surface shows dispersed spalling pits and shear deformation edges, Fig. 4a. A small zone was further enlarged to present a few straight scratches, Fig. 4b, indicating the occurrence of abrasive wear. Figures 4c and 4d show details of the spalling wear. There are a few small fragments with straight edges at the boundary of the spalling pit, showing an evidence of wear by brittle fracture. Such worn surface embrittlement has been confirmed in reciprocating sliding wear of steels [21, 22]. In the bottom of the spalling pit, two graphite flakes were exposed to show multilayer substructures. The appearance of such graphite was seen in the first time, which are consistent to the solidification mode of flake-type graphite that it is known to growth along its (0001) crystalline plane.

The worn disc surface was examined by X-ray diffraction to determine the tribo-oxidation products, as shown in Fig. 5. In addition to the ferrite peaks from the cast iron matrix, two types of iron oxides were detected, namely magnetite Fe_3O_4 and hematite Fe_2O_3 . Obviously the major oxide is magnetite Fe_3O_4 in addition of the remaining ferrite phase. This result is consistent to the analyses of other researchers [16–18]. The tribo-oxidation should be attributed to high temperature of the rubbing surface that the combined high temperature and deformation should be associated with variation of its hardness property.

In Fig. 6, the hardness profile of the polished rubbing surface (seeing Figs. 1c and 1d) and that of the cross-section are illustrated, respectively. In Fig. 6a, the hardness property shows scattering in a large range, giving an average value and deviation of $HV_{0.3} 260 \pm 30$. In Fig. 6b, the rubbing surface shows a relative lower

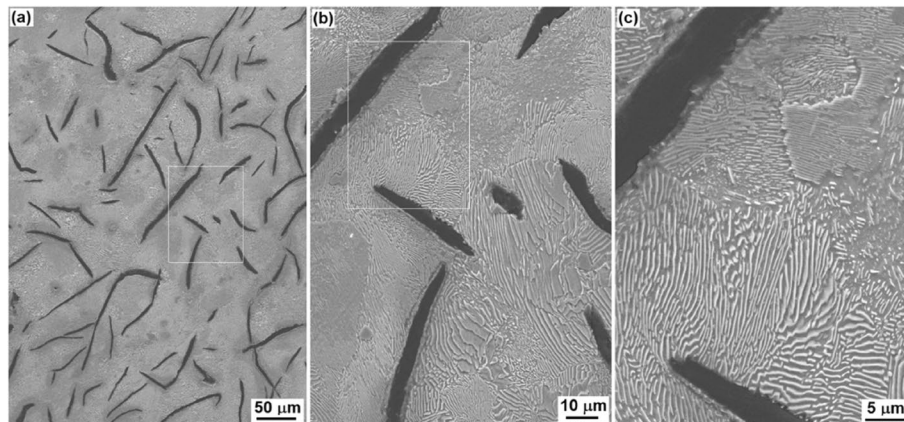


Fig. 3 SEM images taken at a depth of 4 mm beneath the rubbing surface, showing pearlite matrix of the cast iron at various magnifications. Note partial dissolution of the carbide lamella due to the frictional heating

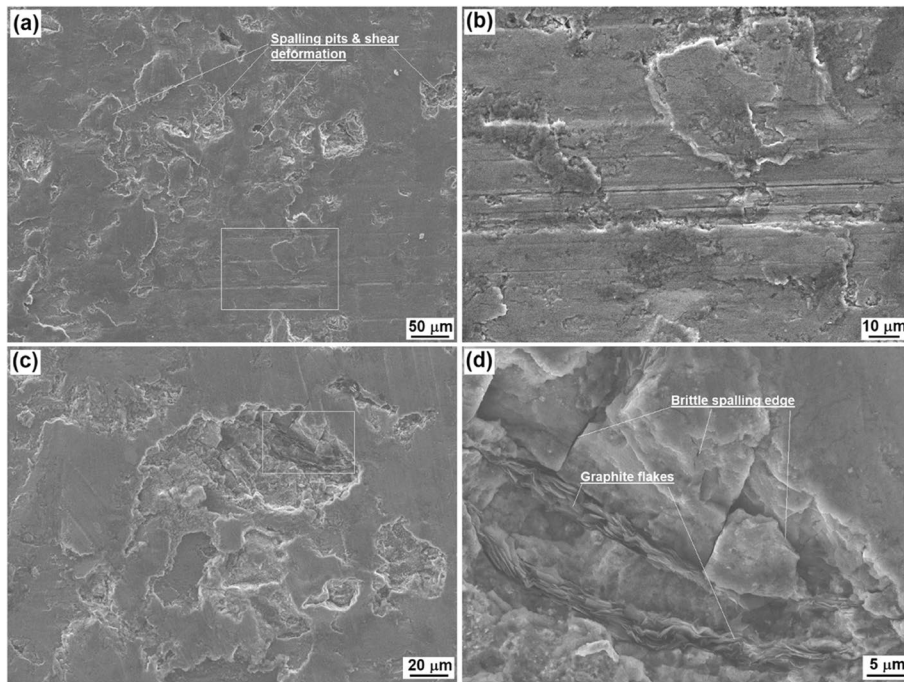


Fig. 4 SEM images of the worn disc surface: **a** a low-magnification view; **b** details of the sliding scratches; **c** an area of spalling pits and **(d)** exposed graphite flakes inside a spalling pit as highlighted in **(c)**

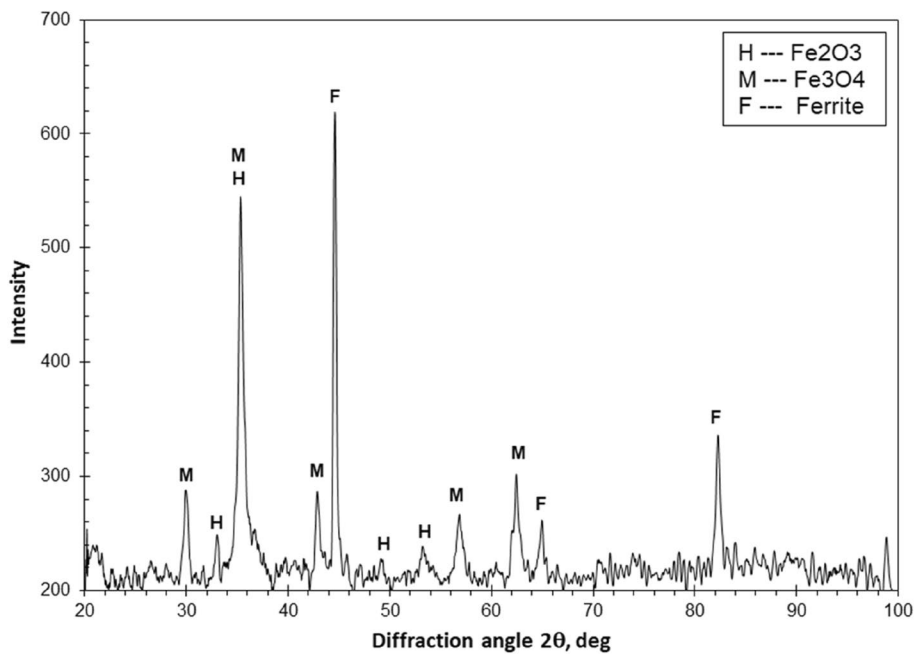


Fig. 5 X-diffraction analysis of the disc worn surface

hardness value and larger data scattering in a depth of 3 mm, namely, HV_{0.3} 247 ± 28. Beyond that depth, the bulk disc shows higher hardness and narrow data

scattering of HV_{0.3} 281 ± 16. It is obvious that the rubbing surface has become substantially softer than the bulk material with a larger scattering of the measured

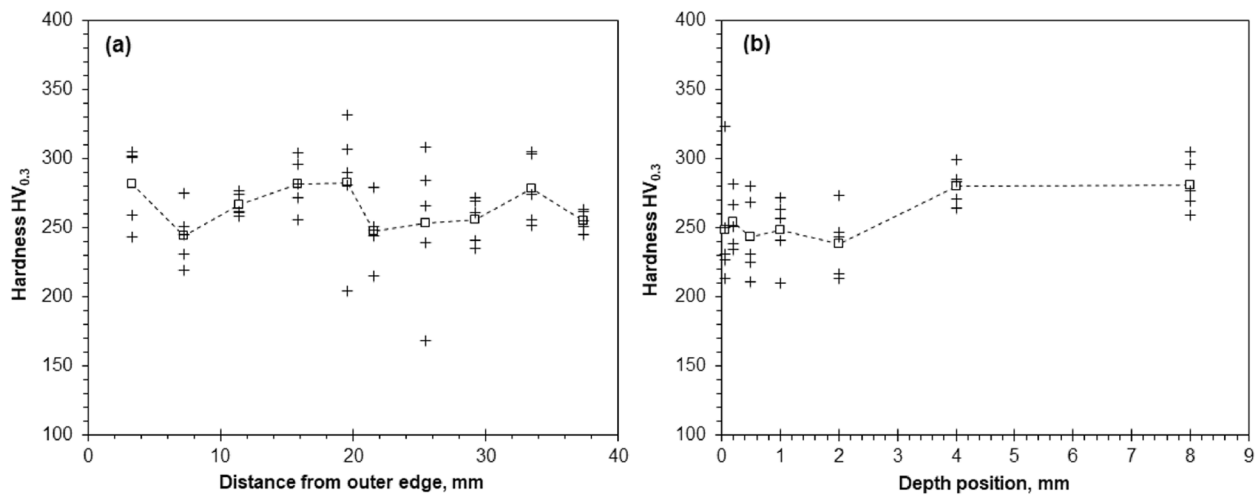


Fig. 6 Microhardness properties of the worn disk: **a** radial profile of hardness in the rubbing surface and **b** subsurface profile of hardness in a vertical cross-section

hardness values. The different hardness property should be attributed to wear induced microstructure evolution.

In addition to these wear features as shown in Fig. 4, the subsurface had been full of thermal crackles, radial cracks and circumferential cracks. These cracks became visible only after removing the rubbing features by a gentle grinding and polishing treatment, as shown in Fig. 1 c-d. These cracking features have been frequently reported not only in grey cast iron brake rotors but also in other materials [6, 7, 9, 11, 15]. The current investigation found that the crack distribution was dense in the middle band of the disc corresponding to the intense rubbing interaction, whereas crack density became much less dense towards the outer circumference where rubbing traces were less. The varying crack density confirms that the predominant cause of the cracking was thermal stresses due to the frictional heating induced hot

shocking for the local temperature at the rubbing contacts can be as high as 800–900 °C [1, 6, 7, 16].

2.3 Cross-sectional characterisation of worn disc

Figure 7 presents optical micrographs of a polished cross-section of the worn disc from its top worn surface to certain depth. The random distribution of graphite flakes is identical to those presented in Fig. 2a. The major feature in Fig. 7 is that a crack perpendicular to the worn surface has been under penetration to a depth of 1.45 mm, as shown in Fig. 7a. Such cracks were observed in other places in which the penetration depths were in a range of 0.2–7 mm. These cracks correspond to the surface network cracks as shown in Fig. 1 c-d. Figure 7b shows an enlarged image highlighted in Fig. 7a. The crack propagation followed the graphite flakes. This finding is consistent to the results published in literature [5, 7]. In addition, some graphite flakes close to the cracks co-exist

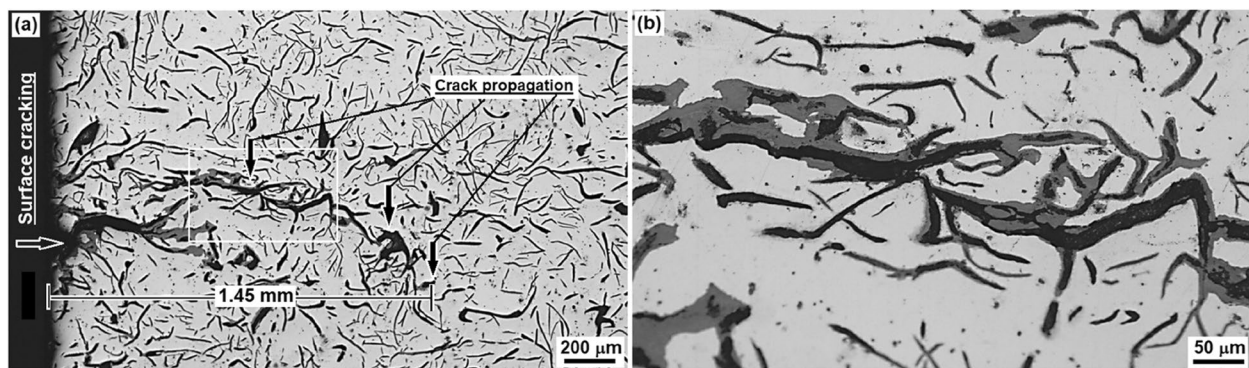


Fig. 7 Cross-sectional optical micrographs showing **a** a surface crack having propagated into a depth in millimetre scale and **b** cracking associated with internal oxidation of ferrite matrix along graphite flakes

with a band showing an intermediate brightness. These bands were assumed to be internal oxidation, which has been confirmed by SEM–EDX analysis as presented later. It seems that the graphite flakes played two roles, namely, the channel for crack propagation and for inward diffusion of oxygen to cause oxidation.

Figure 8 shows the results of cross-sectional microstructure observations using FEG-SEM. Figure 8a is a low-magnification image showing microstructure evolution in a depth beneath the worn surface. The worn surface shows a thin layer differing from the matrix, which is known to be a tribofilm. The disc shows shear deformation in a depth beneath the worn surface. The graphite flakes in close vicinity of the worn surface were all enveloped with a shell having morphology different from the matrix. The carbide in the pearlite matrix had been nodularised no longer showing any lamellar stacking.

Figure 8b shows the matrix microstructure just beneath the worn surface. In the upper part of Fig. 8b, the carbide had completely nodularised where the matrix exhibits a strong orientation indicating the occurrence of shear

deformation. In the lower part, however, there are islands containing extremely fine lamellar carbide. Figure 8c provides more details of these microstructure features at a better spatial resolution. Such mixtures of nodularised carbides and lamellar carbides are also shown in Fig. 8d–e. For example, the area marked ‘I’ shows lamellar carbides and those marked ‘II’ and ‘III’ show nodularised carbides in the ferrite matrix. Obviously, evolution of eutectoid carbide took place in a depth below the worn surface.

Figure 8d and e also show details of a shell enveloping a graphite flake (marked ‘G’). The shell exhibits clearly different morphology as compared to the nearby matrix by showing more large granular particles. There seems a clear boundary of the shell separating it from the matrix, where an artificial dash line has been drawn to show the interface.

The areas of tribofilm, graphite flake and its surrounding shell, and the matrix, as highlighted in Fig. 8a, were analysed by EDX spectroscopy to determine the different chemical compositions of these area. The results are

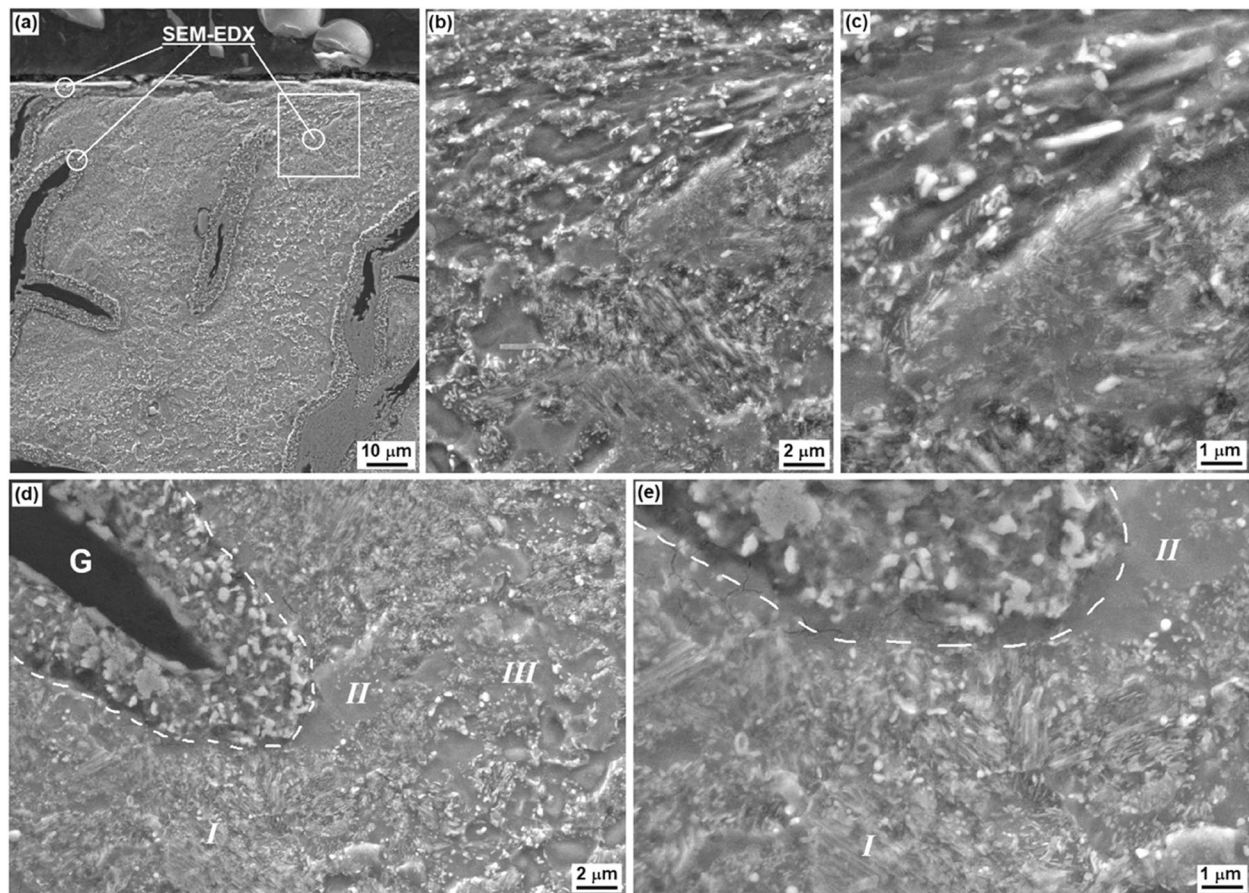


Fig. 8 Cross-sectional SEM images showing wear induced subsurface microstructure evolution: **a** Overview of subsurface microstructure. **b–c** Shear deformation within a depth of 20 μm . **d–e** Internal oxidation adjacent to a graphite flake (marked ‘G’) and nodularised pearlite matrix

presented in Figs. 9 and 10 and Table 1. Figure 9 shows typical spectra of the selected areas whereas quantified results are shown in Table 1. The tribofilm shows a high content of oxygen, followed by the shell of graphite. The

high oxygen content in the tribofilm is consistent with the XRD analysis in its detection of Fe_3O_4 and Fe_2O_3 iron oxides, Fig. 5. To confirm the distribution of oxygen in the subsurface microstructure, 2D mapping was performed,

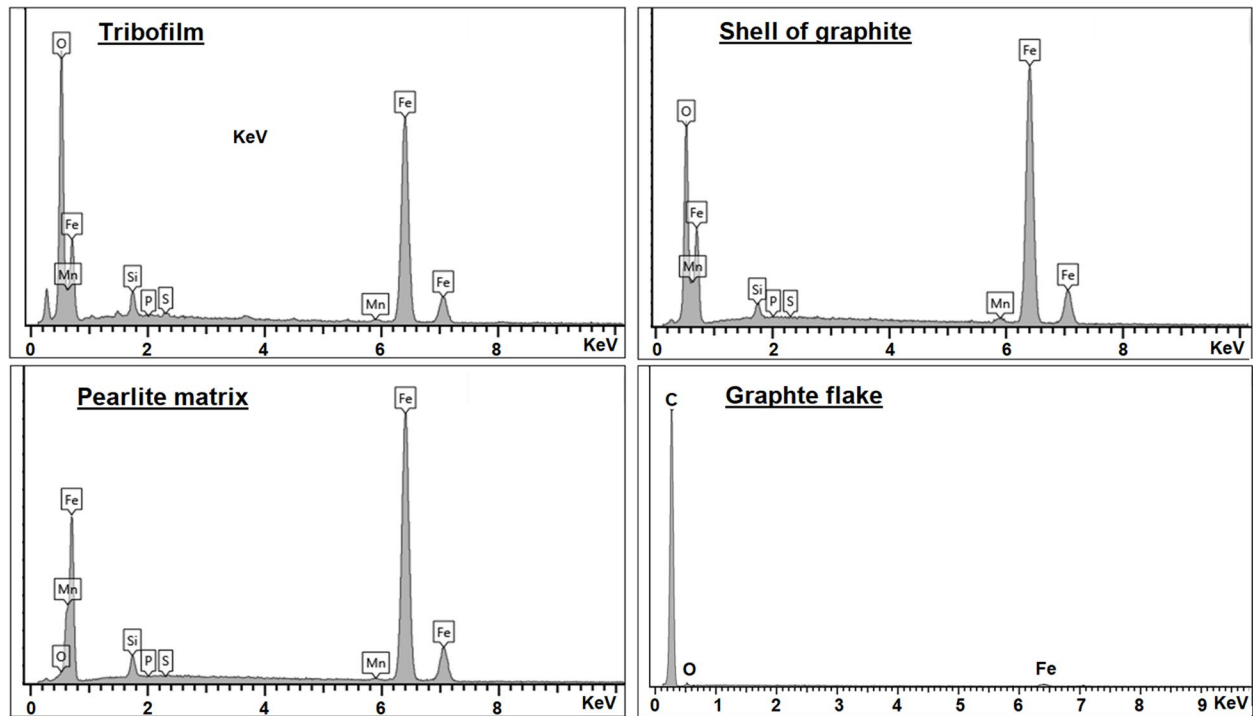


Fig. 9 SEM-EDX spectra acquired in various areas

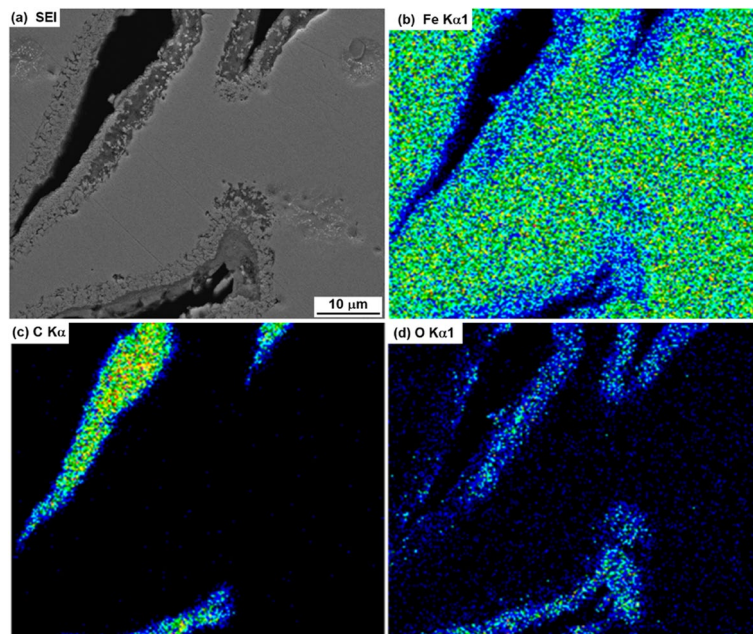


Fig. 10 SEM-EDX mapping analysis showing the internal oxidation

Table 1 Chemical compositions (in at%) of typical areas determined by SEM–EDX analysis

Location	Fe	O	Si	Mn	P	S
Matrix	96.61	0.27	2.54	0.58	0.00	0.00
Shell of graphite	76.10	21.45	1.30	1.10	0.04	0.01
Tribofilm	65.92	30.63	2.29	0.72	0.08	0.36

as shown in Fig. 10. The graphite and matrix show high brightness of C- K_{α} and Fe- $K_{\alpha 1}$, respectively. The graphite shells, on the other hand, show higher brightness of O- K_{α} . These results suggest intense internal oxidation of the pearlitic matrix through the channels provided by the graphite flakes, in addition to the formation of tribofilm on the worn surface top.

In addition to the SEM observations as shown in Figs. 8 and 11 shows the microstructure at depths of 0.5, 1.0 and 2.0 mm beneath the worn surface. The SEM images taken at the depths 0.5 mm and 1.0 mm show similar microstructure features from the graphite flakes enveloped in oxide shells to the nodularised pearlitic matrix, as shown in Fig. 11a-c. Some areas in the matrix

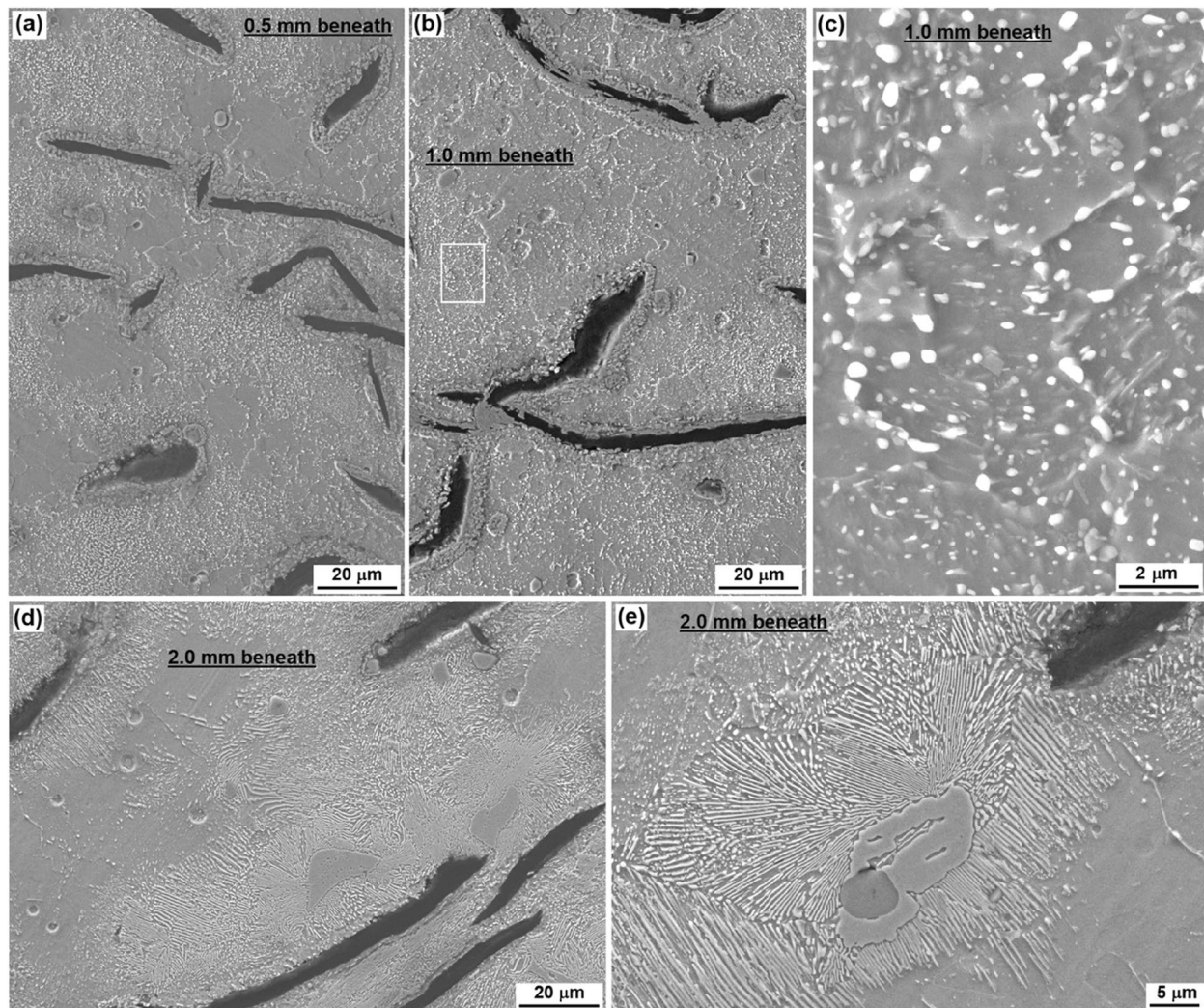


Fig. 11 SEM images showing the microstructure evolution at various depths beneath the rubbing surface: (a) 0.5 mm; b-c 1.0 mm and (d-e) 2.0 mm

are featureless free from any carbide particles, indicating the occurrence of substantial carbide decomposition. In the carbide-containing areas, as shown in Fig. 11c, the carbide particles have been mostly in round shape. Such evolution of the carbide phase is also seen in deeper places as shown in Fig. 11d-e, where both carbide-free areas and carbide modularisation are visible. Figure 11e shows the frontier that the eutectoid lamellar carbides underwent decomposition at the depth of 2.0 mm. These features of carbide decomposition form a striking difference to the microstructure at further depths, e.g., the lamellar pearlitic carbides at the depth of 4 mm as shown in Fig. 5.

To the best of our knowledge, such microstructure evolution of grey cast iron braking discs was not published before. Most previous studies on failures of grey cast iron discs were focused on either the causes of cracking [3, 5–7, 23, 24], the wear induced shear deformation and strain hardening [6, 17, 19, 20, 23] or surface oxidation [16–18]. In current study, the rubbing surface layer has been shown to be extremely deformed (Fig. 8a-c). The rubbing surface, however, did not show any strain hardening. Instead, the rubbing surface showed remarkably lower hardness than the bulk material, as shown in Fig. 6. Such friction induced softening could be attributed to both the formation of gradient microstructure, especially the nodularised eutectoid carbide (Figs. 2c, 8b, c and 11), and internal oxidation along the channels provided by graphite flakes (Figs. 8, 9 and 10). For the former, nodularisation of lamellar eutectoid carbide is known to occur in an annealing process, e.g., at an elevated temperature just below the eutectoid temperature of 723 °C. For the latter, the thick internal oxidised layers were observed only in the subsurface region revealing the localised high temperature. These features provide sufficient evidence to demonstrate the extremely severe heating caused by the braking operations. For this reason, the combined severe shear deformation and frictional heating resulted in surface softening instead of strain hardening. Furthermore, the repeated heating would certainly have caused cyclic thermal stresses. These may have contributed at least partially to the occurrence of the radial cracking failure (Fig. 1a). These explanations are consistent to the finding in Fig. 1c-d that most cracks, including chackles and radial cracks, were formed in the middle band of the braking disc where the cyclic rubbing took place mostly.

3 Conclusions

The rubbing surface of a failed braking disc made from grey cast iron was analysed extensively to investigate the failure mechanisms. The experimental results lead to the following conclusions.

- 1) The disc showed spalling wear as a result of severe plastic deformation and embrittlement as well as marginal abrasive wear. Tribo-oxidation was also found to lead to the formation of tribofilms dominated by magnetite Fe_3O_4 and hematite Fe_2O_3 .
- 2) The disc also showed extensive cracking failure as featured by large radial cracks and a dense distribution of thermal crackles and circumferential cracks.
- 3) The rubbing surface showed a gradient microstructure indicating evolution of the pearlitic matrix and graphite flakes, including extremely serious plastic deformation of the ferritic based matrix, completely nodularised and partially dissolved eutectoid carbide and internal oxidation of the ferritic matrix. The graphite flakes were found to be the channel both for propagation of surface cracks and inward diffusion of oxidising species.
- 4) The worn surface did not show any strain hardening. Instead, the friction induced microstructure evolution resulted in decreased surface hardness to $\text{HV}_{0.3}$ 247 in a depth of 3 mm as compared to $\text{HV}_{0.3}$ 284 of the bulk cast iron.

Acknowledgements

This research was partially funded by in the European Regional Development Fund of European Union in the title 'Sheffield Innovation Programme' with the series number 28R18P02582.

Authors' contributions

All authors contributed to this paper: QL, SJ and NK in funding issue, XW and JS in sample supplying and visual inspection, QL and XG in laboratory study and results analyses, QL and NF in project management, QL in manuscript drafting.

Funding

The research was partially funded by European Union in the European Regional Development Fund.

Availability of data and materials

The data and material presented in this paper are available.

Declarations

Competing interests

The authors have no competing interests.

Received: 8 October 2023 Revised: 4 December 2023 Accepted: 7 December 2023

Published online: 10 January 2024

References

1. Cueva G, Sinatora A, Guesser WL, Tschiptschin AP (2003) Wear resistance of cast irons used in brake disc rotors. *Wear* 255:1256–1260
2. Li Z, Han J, Li W, Pan L (2014) Low cycle fatigue of Cr-Mo-V low alloy steel used for railway brake discs. *Mater Des* 56:146–157
3. Pevac M, Oder G, Potrc I, Sraml M (2014) Elevated temperature low cycle fatigue of grey cast iron used for automotive brake discs. *Eng Fail Anal* 42:221–230

4. Mulani SM, Kumar A, Shaikh HNEA, Saurabh A, Singh PK, Verma PC (2022) A review on recent development and challenges in automotive brake pad-disc system. *Mater Today: Proceedings* 56:447–454
5. He G, Pan A, Wang C, Ouyang Z, Xu X, Jiang P, Zhang Y, Jin H, Wu W (2023) Failure analysis of inner wall of X-10 brake discs for urban rail vehicles. *Eng Fail Anal* 146:107067
6. Mackin TJ, Noe SC, Ball KJ et al (2002) Thermal cracking in disc brakes. *Eng Fail Anal* 9:63–76
7. Bagnoli F, Dolce F, Bernabei M (2009) Thermal fatigue cracks of fire fighting vehicles gray iron brake discs. *Eng Fail Anal* 6:152–163
8. Samec B, Potrc I, Sraml M (2011) Low cycle fatigue of nodular cast iron used for railway brake discs. *Eng Fail Anal* 18:1424–1434
9. Yang Z, Han J, Li W, Li Z, Pan L, Shi X (2013) Analyzing the mechanisms of fatigue crack initiation and propagation in CRH EMU brake disc. *Eng Fail Anal* 34:121–128
10. Mohammadnejid A, Bahrami A, Goli M, Nia HD, Taheri P (2019) Wear induced failure of automotive disc brakes - A case study. *Materials* 12:4214
11. Lu C, Shen J, Fu Q, Mo J (2023) Research on radial crack propagation of railway brake disc under emergency braking condition. *Eng Fail Anal* 143:106877
12. Straffelini G, Maines L (2013) The relationship between wear of semi-metallic friction materials and pearlitic cast iron in dry sliding. *Wear* 307:75–80
13. Verma PC, Ciudin R, Bonfanti A, Aswath P, Straffelini G, Gialanella S (2016) Role of the friction layer in the high-temperature pin-on-disc study of a brake material. *Wear* 346–347:56–65
14. Riahi AR, Alpas AT (2003) Wear map for grey cast iron. *Wear* 255:40–409
15. Harada N, Takuma M, Tsujikawa M, Higashi K (2013) Effects of V addition on improvement of heat shock resistance and wear resistance of Ni-Cr-Mo cast steel brake disc. *Wear* 302:1444–1452
16. Konig T, Kimpel T, Kurten D, Kailer A, Dienwiebel M (2023) Influence of atmospheres on the friction and wear of cast iron against chromium plated steel at high temperatures. *Wear* 522:204695
17. Osterle W, Klob H, Urban I, Dmtriev AI (2007) Towards a better understanding of brake friction materials. *Wear* 263:1189–1201
18. Hinrichs R, Vasconcellos MAZ, Osterle W, Prietzel C (2011) A TEM snapshot of magnetite formation in brakes: The role of the disc's cast iron graphite lamellae in third body formation. *Wear* 270:365–370
19. Prasad BK (2011) Sliding wear response of a grey cast iron: Effects of some experimental parameters. *Tribol Int* 44:660–667
20. Rynio C, Hattendorf H, Klöwer J, Eggeler G (2014) The evolution of tribolayers during high temperature sliding wear. *Wear* 315:1–10
21. Luo Q, Zhu J (2022) Wear property and wear mechanisms of high-manganese austenitic Hadfield steel in dry reciprocal sliding. *Lubricants* 10:37
22. Luo Q, Kitchen M, Li J, Li W, Li Y (2023) Experimental investigation on the spalling failure of a railway turnout made from Hadfield steel. *523:204779*
23. Boniardi M, D'Errico F, Tagliabue C, Gotti G, Perricone G (2006) Failure analysis of a motorcycle brake disc. *Eng Fail Anal* 13:933–945
24. Awe SA (2022) Premature failure of an automobile brake disc: Effect of non-metallic inclusions. *Eng Fail Anal* 137:106263

Publisher's Note

Springer Nature remains neutral with regard to jurisdictional claims in published maps and institutional affiliations.